

Article

A Novel and Self-Calibrating Weighing Sensor with Intelligent Peristaltic Pump Control for Real-Time Closed-Loop Infusion Monitoring in IoT-Enabled Sustainable Medical Devices

Chiang Liang Kok ^{1,*}, Chee Kit Ho ², Yuwei Dai ¹, Teck Kheng Lee ³, Yit Yan Koh ¹ and Jian Ping Chai ¹

¹ College of Engineering, Science and Environment, University of Newcastle, Callaghan, NSW 2308, Australia

² Engineering Cluster, Singapore Institute of Technology, Singapore 138683, Singapore

³ Institute of Technical Education College Central, Singapore 567720, Singapore

* Correspondence: chiangliang.kok@newcastle.edu.au

Abstract: Technological advancements are propelling medical technology towards automation through the application and widespread use of automatic control, sensing, and Internet of Things (IoT) technologies. Currently, IoT technology has been extensively applied in medical devices, aiming to ensure patient safety through more real-time detection and more effective management. In the monitoring of intravenous infusion, accurately sensing the infusion conditions in real time is particularly important. This article introduces a low-cost smart infusion device based on IoT technology, which controls the infusion rate with a peristaltic pump and monitors the volume of fluid delivered. It uses an improved, self-calibrating weighing sensor to achieve the real-time closed-loop control of the flow rate, ensuring patient safety. Additionally, the Blynk dashboard can be used for monitoring and controlling the flow rate and infusion volume.

Keywords: IoT device; medical device; flow rate control; weight sensor; IoT sensor; ESP32; smart IoT



Citation: Kok, C.L.; Ho, C.K.; Dai, Y.; Lee, T.K.; Koh, Y.Y.; Chai, J.P. A Novel and Self-Calibrating Weighing Sensor with Intelligent Peristaltic Pump Control for Real-Time Closed-Loop Infusion Monitoring in IoT-Enabled Sustainable Medical Devices.

Electronics **2024**, *13*, 1724. <https://doi.org/10.3390/electronics13091724>

Academic Editor: Hyun Jae Baek

Received: 3 April 2024

Revised: 25 April 2024

Accepted: 27 April 2024

Published: 30 April 2024



Copyright: © 2024 by the authors. Licensee MDPI, Basel, Switzerland. This article is an open access article distributed under the terms and conditions of the Creative Commons Attribution (CC BY) license (<https://creativecommons.org/licenses/by/4.0/>).

1. Introduction

Intravenous infusion is a very common treatment method used to inject fluids, medication, or nutrition directly into a patient's veins [1–3]. The process often requires simultaneous verification by two people, consuming a significant amount of manpower [4]. At the same time, air embolism, blood reflux, underdosing, and overdosing of medication are widely discussed issues in traditional intravenous infusion [5–7]. Injecting too many bubbles into a patient's body can cause air embolism, leading to an increased cardiac load and discomfort for the patient, and can even be fatal in severe cases [8]. Incorrectly set heights of the infusion set or the replacing of bottles in an untimely manner when the fluid is about to run out can lead to blood reflux into the infusion pipe, potentially causing local swelling and infection [9]. The overdosing and underdosing of medication are mostly due to human factors, generally arising from medical personnel not correctly preparing medications or setting the flow rate correctly in those treatments they are not familiar with [5,10]. There are still few cases due to errors in the medication delivery device [11]. By introducing IoT technology, the process can be changed to one-nurse on-site verification and the other remote verification to reduce the unnecessary waste of human resources. Meanwhile, IoT infusion devices can rely on various sensing and control modules to ensure accurate dosing and avoid air embolism, blood reflux, overdosing, and underdosing issues [12–15]. An infusion device using a closed-loop controlled stepper-motor-driven peristaltic pump can control the infusion speed and total volume to prevent blood reflux due to low fluid levels and non-human factors causing overdosing and underdosing. For such devices, the accurate monitoring of the total amount of medication delivered and the real-time flow rate are particularly important. Current market products using infusion pumps mostly employ servo stepper motors to drive a plunger pushed by a shaft, which is

zeroed by a photoelectric limit switch, to accurately deliver and calculate the flow rate of fluid [16,17]. This method has a very low error and can achieve a high accuracy but is complex to manufacture and adds about \$30 to the cost over traditional stepper motor infusion pumps. Some low-cost solutions rely on cost-effective opposed photoelectric sensors for monitoring [18]. These sensors have a failure rate of less than 0.5%, but manufacturing tolerances of the drip chamber and air valve, as well as environmental factors like temperature and air pressure, can introduce significant variations, with studies mentioning a median rate error reaching 5%, leading to a substantial cumulative error in the final volume [19]. In one other work, electrostatic capacitive sensors have been used by reading the change in capacitance caused by droplets passing through electrodes placed on the drip chamber to calculate the volume of each droplet [20]. This method can achieve a less than 3% error per measurement, and, since the noise sources are relatively random, it does not result in a significant cumulative error, thus resulting in a minimal final volume error. However, this method is currently expensive, costing around \$100, and the modulation noise caused by the horizontal movement of the drip chamber is difficult to filter effectively without adding additional sensors, like a three-axis accelerometer. Weight sensors and ultrasonic sensors are common IoT sensors that have been used in some studies to detect the weight or fluid level, thereby determining the infused and remaining fluid volume [8,21]. Additionally, visual methods have been used to monitor fluid levels or droplets [22–24]. These methods generally have a lower accuracy and higher cost. Using a load cell to determine the remaining fluid volume is a very cost-effective method, commonly relying on the change in resistance caused by the strain to sense weight, typically using an HX711 ADC and a single-point load cell, with the center of the strain area of the load cell fitted with four-wire strain gauges [8,25]. The change in differential voltage produced on the Wheatstone bridge due to the resistance change read by the HX711 ADC is used to determine the weight. This method has an error margin that meets the basic needs of intravenous infusion but usually cannot achieve the closed-loop control of the infusion pump flow rate. This paper introduces an infusion device that achieves the closed-loop control of the peristaltic pump through a weighing sensor, by incorporating an unloaded load cell as a reference and an IIR digital filter, enabling the monitoring of the real-time flow rate using a weight sensor, thus achieving the closed-loop control of the infusion flow rate. The following points summarize the uniqueness and innovation of this study:

- A set of infusion equipment was designed, using a closed-loop controlled stepper-motor-driven peristaltic pump to achieve precise control of the flow rate and infusion volume;
- A self-calibration process was designed for the load cell to achieve calibration during use, and a filter was configured for the weighing sensor to meet the needs of measuring the flow rate in order to perform closed-loop control in intravenous infusion applications.

2. Materials and Methods

2.1. Overview: System Block Diagram

Figure 1 provides the overall workflow diagram delineating the three different modules of the project: microcontroller algorithm, control system, and Internet of Things (IoT).

Medical devices require higher safety and reliability standards; this IoT system is designed to ensure it can run for a period even without network and power supply. It also allows complete control of the infusion system via physical user interface on device. When the infusion system encounters a power outage or goes offline, the IoT terminal can detect it instantly, ensuring that any anomalies can be addressed promptly.

The microcontroller algorithm section acts as the physical interface between the user and the hardware. An ESP32 microcontroller is used in this project. The user can provide the prescribed data (target volume, target flow rate, and solution type) for the patient through the microcontroller. After that, the in-built flow rate algorithm will calculate the suitable rotation rate for stepper motor to achieve the targeted specifications from

prescribed data. The calculated flow rate will act as the target reference for the control system of the drug infusion device. The real-time infused volume obtained from sensors will be displayed out for real-time monitoring. The control system manages and regulates the drug infusion device to achieve the desired flow rate. The control system achieves this through a closed-loop feedback design, which is a process designed to maintain the flow rate at the desired set point from the program algorithm set by the user. One key application of the project is to provide healthcare practitioners with the ability to perform accurate and safe administration of drugs remotely. Therefore, a web dashboard will be designed to interact with the drug infusion device via a personal computer or an application for mobile phone. Users can provide the prescribed data to the device and monitor the device from anywhere in the world through Wi-Fi networks. The front-end development using Blynk interface view interacts with the server. The back-end development using Blynk Cloud Server will organize and communicate all the data in the server obtained from the drug infusion device via a Wi-Fi module and the front-end. The uninterruptible power supply acts as the portable or backup power source for the infusion device. The UPS system also keeps the infusion device operating while charging without any interruptions.

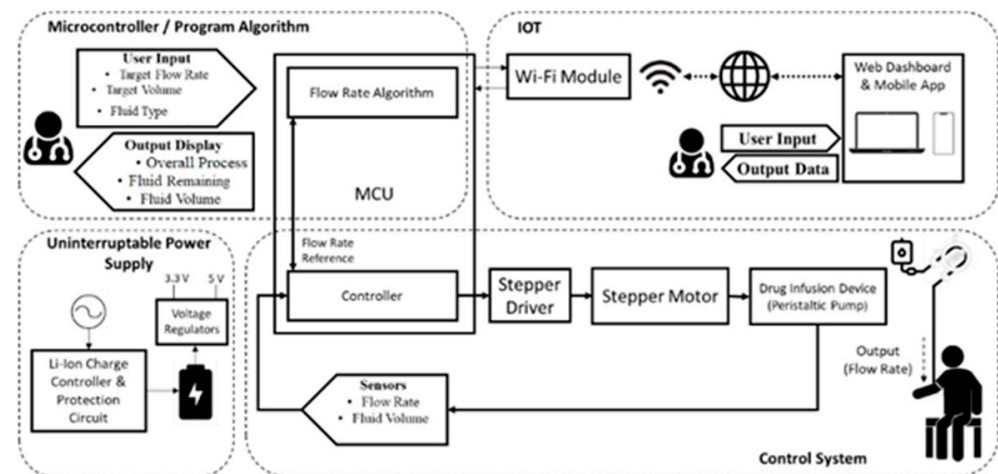


Figure 1. Overall block diagram of the project [26].

2.2. Weight Sensors in Infusion System

Weight sensors are widely used in IoT devices. The most common type of weight sensor is the strain gauge load cell. Load cells are mainly categorized into several types: single point, bending beam, double shear beam, and S-type. Among these, the S-type load cell is commonly used for hanging scales, and the bending beam load cell is often applied in scenarios with large loads. Single-point load cells are cheapest but have poor anti-interference capability, being sensitive to placement position without quadrangle calibration and environmental vibrations. These interference factors have a lesser impact on double shear beam load cells, which can also be designed for larger loads, but double shear beam load cells are more expensive and may require more ADC channels [27]. Calibration should apply for infusion system since different solutions used in medical infusions have varying densities. Fluid in infusion is classified as isotonic, hypotonic, hypertonic, and colloidal solutions [28]. For isotonic, hypotonic, and hypertonic infusions, the medication concentration is typically low enough not to significantly affect the fluid's properties [29–32]. Thus, calibration only needs to be performed for the type of solution in common environments, such as at 20 °C and standard atmospheric pressure. However, for colloidal fluids, data need to be adjusted for each type separately. Different temperatures can also cause changes in density, but, since infusion therapy focuses more on the molar quantity of the drugs dispersed in the solution, if the density of the fluid increases or decreases due to temperature changes, the per volume molar quantity will correspondingly increase or decrease [33,34]. Therefore, it is more reasonable not to compensate for temperature and directly use the mass corre-

sponding to the type of solution as the basis for determining whether an adequate amount of drug has been administered.

3. Design and Development

3.1. Reading Drift of the Strain Gauge Load Cell Weight Sensor

The sensor employs a 1 kg full-scale single-point parallel beam load cell to achieve lower costs. The load cell has four wires leading out: two connect to the excitation source, and two connect to the positive and negative input of the ADC preamplifier. Two parallel Acrylic plastic plates are fixed on both sides of the load cell as the base and upper platform. The HX711 24-bit ADC module is used to read load data and communicate with the microcontroller. This ADC includes a ± 1.25 V built-in reference voltage, a built-in regulated source as the excitation voltage for the strain gauges and amplifier with three adjustable gains of 32, 64, and 128 times for amplifying the output voltage of the load cell. It also allows setting two sampling rates of 10 Hz and 80 Hz. Due to its features and low cost, it is commonly used as the ADC for weight sensors. The above materials form a weighing platform. Several weights, calibrated for actual weight using a milligram scale, are used as references to calibrate the load cell. When testing the weighing platform, it must first be calibrated. The HX711 module is powered by a 5 V adjustable power supply, with its gain set to 128 and sampling rate set to 10, giving an average reading of ten measurements per second. Since the module does not have an anti-aliasing filter on board, two of the 100 μ F filter capacitors are added to the positive and negative analog input of HX711 module. Considering the 1000 Ω output resistor of load cell, the RC filter cut-off frequency is approximately 3.15 Hz. The calibration weights range between 0–700 g in 50 g steps. The actual weight of the weights is read by a milligram scale and placed at the center of the load cell. The average of ten sampling values is printed via the serial port, and then an average of these ten values is taken to obtain the calibration raw data. The load cell is a linear sensor, and, excluding the zero point, the data are fitted with a linear equation to minimize the mean square error, obtaining a scale factor of 1086.65. Taking the zero-point reading as the offset, the calibration curve and data points are shown in Figure 2.

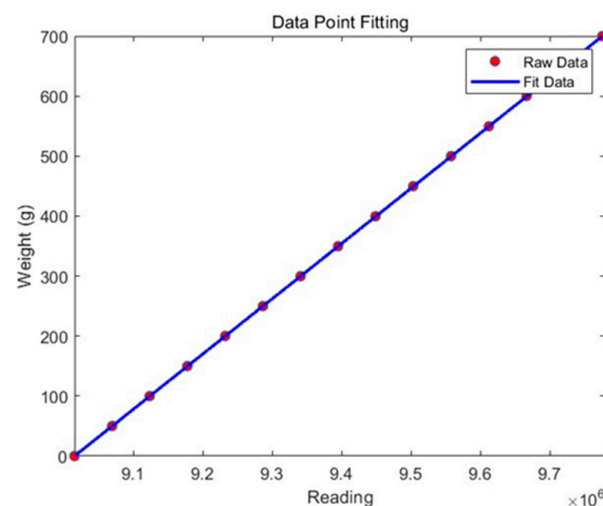


Figure 2. Weight scale calibration condition.

When a total of 699.82 g weights is placed at the center of the calibrated and scale-factor-adjusted weight sensor's load cell, the drift of the weight sensor under this load and the impact of the variation on the overall closed-loop system volume accuracy and flow rate accuracy are shown in Figure 3. The variance of the drift for different varying periods is shown in Figure 4, indicating a significant increase in variance after 1000 s.

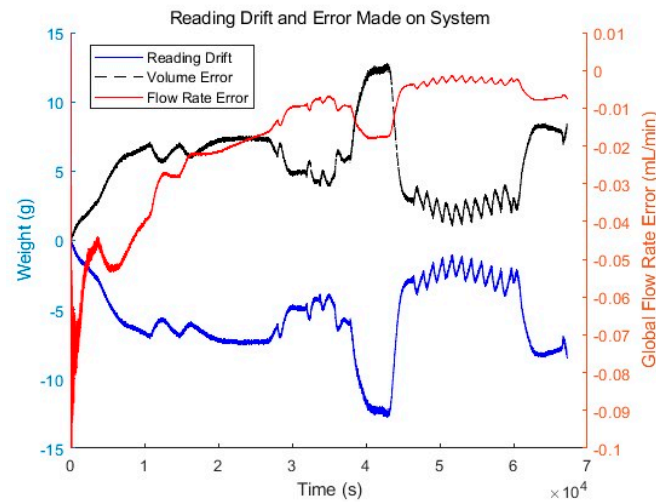


Figure 3. Reading drift vs. time graph.

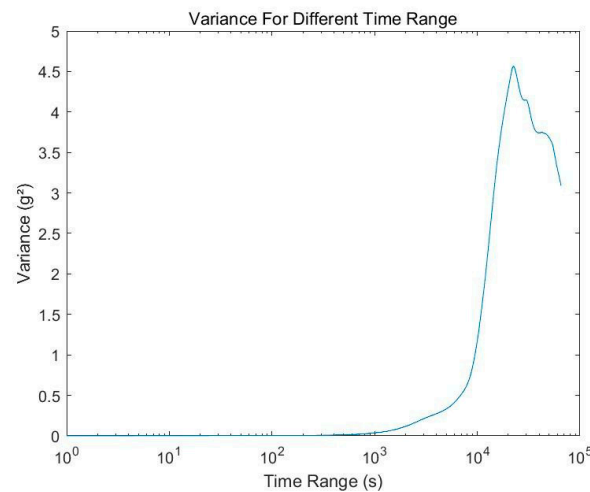


Figure 4. Variance vs. time range.

In most discussions about the drifting of load cells, the primary cause is attributed to temperature changes. Temperature changes can lead to changes in the mechanical stress of the load cell, altering the strain and, thus, changing the readings [35,36]. One article also mentions that the temperature drift of the resistors across the ADC input can increase the drifting of the weight sensor readings [37]. Electromagnetic interference and power supply integrity might also affect drift [38]. ADI's high-performance, low-cost weight scale design reference mentions that the ADC chip contributes to the primary random noise and a certain drift with temperature. The load cell can drift over time under load, independent of temperature, caused by creep [39]. Creep is the steady and slow deformation of materials under a constant static load. Creep causes an increase in the strain of the load cell, thereby making the readings larger [40]. ADI's experiments also show that using lower sampling rates and higher gains helps reduce rms noise. These reasons for drift in readings will be reflected in changes in the sensor's offset. The drift of the weight sensor's readings could also be caused by changes in sensor sensitivity or amplifier gain. The data sheet for the load cell indicates that its sensitivity changes by less than 0.15%/10 °C with temperature. The built-in amplifier gain change of the HX711 is less than 5 ppm/°C. The former would manifest as a change in the scale factor, while the latter would cause changes in both the scale factor and offset. Therefore, two different self-calibration methods were designed for the offset and scale-factor-induced drifting.

3.2. Drifting Calibration Method Based on Drifting Composition

For the self-calibration of the load cell's offset drift, the designed method uses the drift of the no-load reading of another identically designed load cell as a reference to calibrate the zero point of the weight sensor loaded with 699.82 g, with the sketch map as shown in Figure 5. Figure 6 shows the drift of the reading when the weight sensor loaded with 699.82 g is calibrated once every 15 min with the average value of 10 s from another unloaded load cell of the same model powered by the same power supply in the same environment.

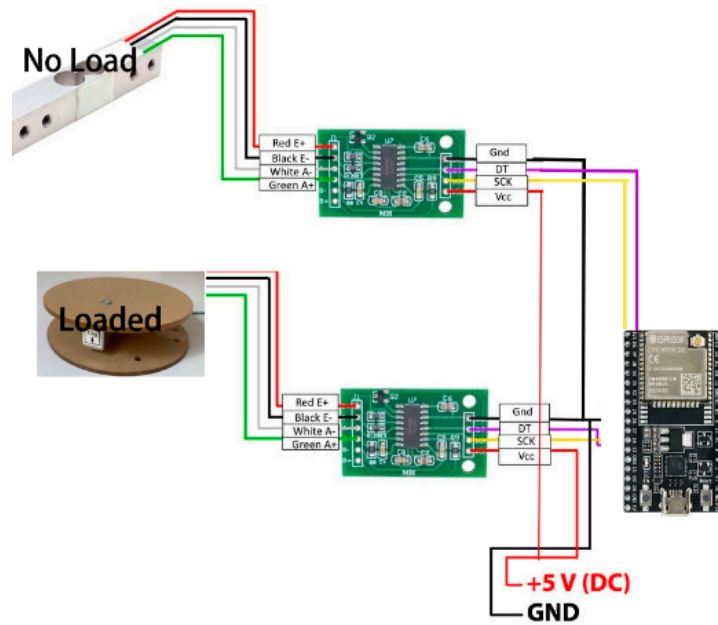


Figure 5. Offset calibration setup.

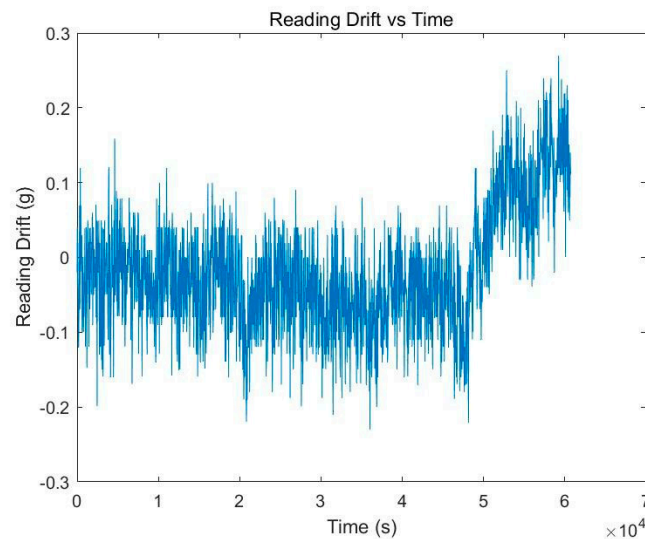


Figure 6. Drift vs. time with offset calibration.

It is apparent that, after incorporating the calibration mechanism, the sensor's drift significantly reduces compared to the drift mentioned previously. This indicates that almost all the offset comes from the noise in the environment affecting similarly designed sensors consistently, and the offset seems not to have many components other than the offset. However, from about 5×10^4 s, the offset begins to show a significant upward trend, which could be the shift caused by creep mentioned above.

In addition to the calibration method mentioned above, there was an attempt to introduce a calibration method for the scale factor to eliminate the impact such as temperature on the scale factor. However, the sensor's repeatability error is too large, around ± 0.15 g. This far exceeds the scale factor shift caused by every 10°C deviation noted in the data sheet, suggesting that, with the calibration method for scaling factors, additional uncertainty was introduced, higher than the temperature drift error being calibrated. For a self-calibration method for the scale factors introduced, drift vs. time is shown in Figure 7, and the corresponding variance vs. time is shown in Figure 8. On the same timescale, the variance is even worse than the variance is without self-calibration.

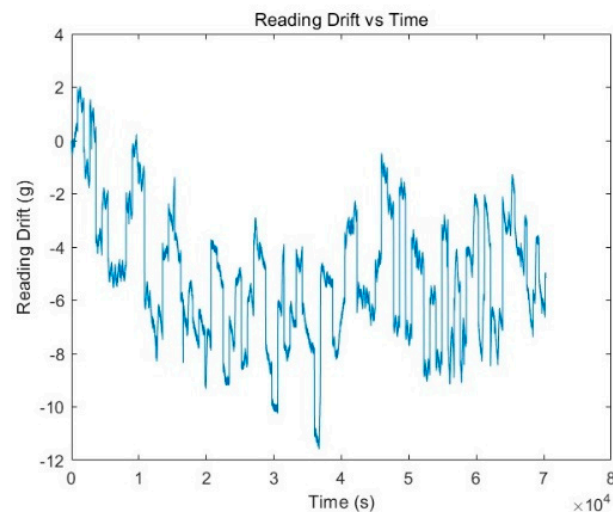


Figure 7. Reading drift vs. time with scale factor calibration.

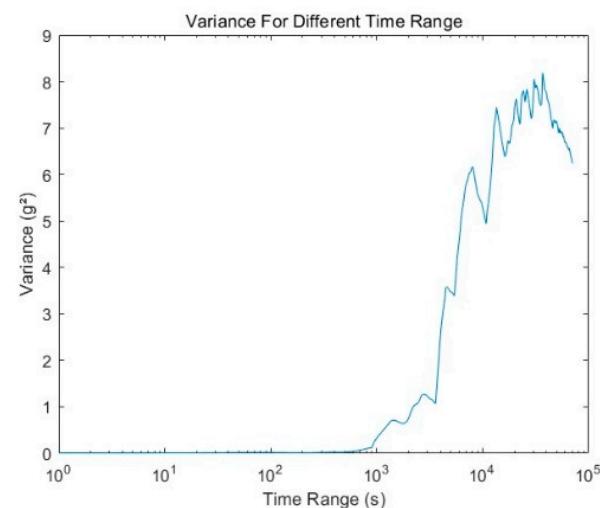


Figure 8. Variance vs. time range.

3.3. Closed-Loop Control of the Stepper Motor Peristaltic Pump

The type of peristaltic pump design that will be considered in this project is the roller-type peristaltic pump. It generates flow by deforming the infusion pipe and forces the fluid to flow in one direction. This pump design isolates the fluid from the mechanical parts of the pump which prevents any contamination to the flowing fluid in the pipe. The one requirement for this roller-type peristaltic pump is that the infusion pipe material must be flexible or elastomeric. The conceptual design of this stage is compatible with an infusion pipe that is 4.5 mm in diameter. The 3D printable parts for the pump are illustrated in Figure 9. Figure 10 listed the measurements of the fluid displacement vs. revolutions of the

peristaltic pump and the fitted data, while the fluid displacement per revolution is set to 0.167 mL/revolution.

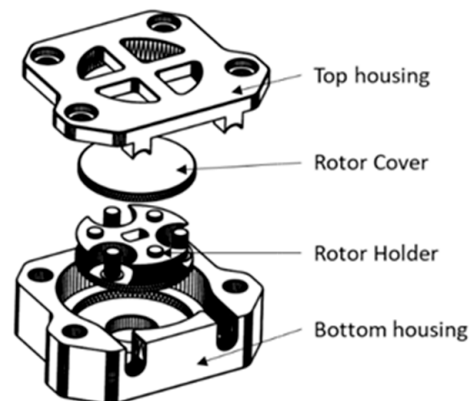


Figure 9. CAD model for the peristaltic pump.

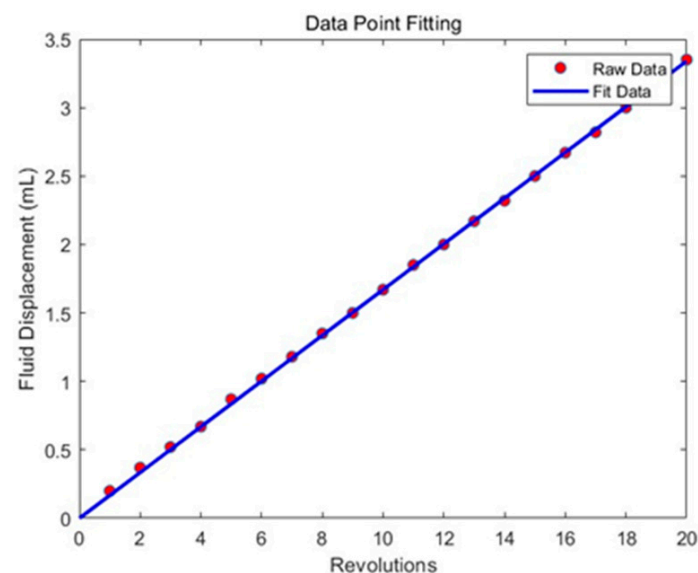


Figure 10. Fluid displacement per revolution fitting result.

From the experiment, a 5V-28byj-48 stepper motor can rotate smoothly against the surface of the silicone pipe without being out of step at 0–16 rpm. However, due to the implementation of the control system, the applicable input operating speed should be decreased to reduce the chances of saturation. To achieve the closed-loop control of the infusion flow rate, the accurate reading of the flow rate is necessary. Therefore, it is essential first to filter the readings from the weight sensor.

Table 1 above presents some publicly available information from hospitals regarding infusion dosage and flow rate [29–32]; it is evident that the peristaltic pump can fully meet the needs of common treatment projects. The fastest treatment procedure in intravenous infusion therapy also requires at least 60 min to complete. The corresponding bandwidth is $\omega = 0.0008767$ Rad/s. For an infusion volume of 50 mL, the stepper motor's maximum flow rate bandwidth of $\omega = 0.0028$ Rad/s. Appropriately configuring a filter can effectively reduce the modulation noise from the platform vibration, EMI, and power source interference. An infinite impulse response (IIR) filter is a commonly used digital signal processing filter that can achieve performance similar to an analog filter with very low computational expense. Its expression is as follows [41]:

$$y[n] = \frac{1}{a_0} \left(\sum_{i=0}^P b_i x[n-i] - \sum_{j=1}^Q a_j y[n-j] \right) \quad (1)$$

where $x[n]$ is the input signal, $y[n]$ is the output signal, a_i are the feedback filter coefficients, b_i are the feedforward filter coefficients, Q is the feedback filter order, and P is the feedforward filter order.

Table 1. Guidelines for intravenous medications about dosing rate.

Drug Name	Dosing Rate	Flow Rate (For 65 kg Adult)
Abciximab	0.125 µg/kg/min	0.226 mL/min
Amiodarone	1 mg/min	0.556 mL/min
Bumetanide	0.25–0.5 mg/h	6.25–12.5 mL/h
Cisatracurium	0.15–0.2 mg/kg/h	12.189–16.25 mL/h
Dexmedetomidine (Precedex)	0.2–1.4 µg/kg/h	3.25–22.75 mL/h
Diltiazem (Cardizem)	5–15 mg/h	5–15 mL/h
Dobutamine (Dobutrex)	2.5–20 µg/kg/min	0.081–0.65 mL/min
Dopamine	2–20 µg/kg/min	0.081–0.812 mL/min
Epinephrine	0.05–0.45 µg/kg/min	0.163–1.463 mL/min
Esmolol	50–300 µg/kg/min	0.325–1.95 mL/min
Fentanyl	25–150 µg/h	2.5–15 mL/h
Heparin	13 units/kg/h	8.45 mL/h
Insulin (Regular)	Based upon blood glucose level—follow protocol	-
Isoproterenol	0.5–20 µg/min	0.031–1.25 mL/min
Lidocaine	1–4 mg/min	0.25–1 mL/min
Magnesium	1000 mg/h	50 mL/h
Morphine	1–10 mg/h	1–10 mL/h
Nicardipine	5 mg/h	50 mL/h
Potassium Chloride	≤10 mEq/h	≤100 mL/h
Propofol (Diprivan)	5–75 µg/kg/min	0.033–0.488 mL/min
Vasopressin	0.04 units/min	0.1 mL/min

The sampling period of the IIR filter is set to the reading frequency, which is 1 s, and a first-order Butterworth filter with a bandwidth of 10 times the maximum infusion bandwidth is selected. Its transfer function is transformed into an IIR filter:

$$H(z) = \frac{0.0422 + 0.0422z^{-1}}{1 - 0.9157z^{-1}} \quad (2)$$

resulting in $a = [1, -0.9157]$, and $b = [0.0422, 0.0422]$. Under this filter configuration, at the maximum bandwidth $\omega = 0.0028$ Rad/s, the error is -0.02% , with a phase lag of 0.01 Rad, which is equivalent to a 4 s reading delay. This meets the design requirements. The filter is delayed for one second after the stepper motor peristaltic pump is started, in order to wait for the pump to reach a steady state. Then, the filter is initialized with the target flow rate as the initial state, and then starts operating. At a speed of 16 rpm, defining the input as the rpm speed and the output as the flow rate in mL/min, its transfer function is

$$G(s) = \frac{65}{s + 390} \quad (3)$$

In the time dimension of minutes, the transfer function of the mentioned filter is

$$G(s) = \frac{1.68}{s + 1.68} \tag{4}$$

Since the weight sensor can directly read the total injection amount to determine whether to stop, without considering cumulative errors, it is only necessary to make the flow rate as accurate as possible and reduce the impact of transient noise. Therefore, PI control is chosen. Adjusting PI parameters through the above transfer functions, the PI parameters are adjusted to:

- $K_p = 8.5$;
- $K_i = 26$.

Under these parameters, the closed-loop system rise time is 3.66 min, and the settling time is 12.56 min.

3.4. IoT User Interface

Figure 11 shows the block diagram about the calibration method mentioned above and how it integrates with the IoT.

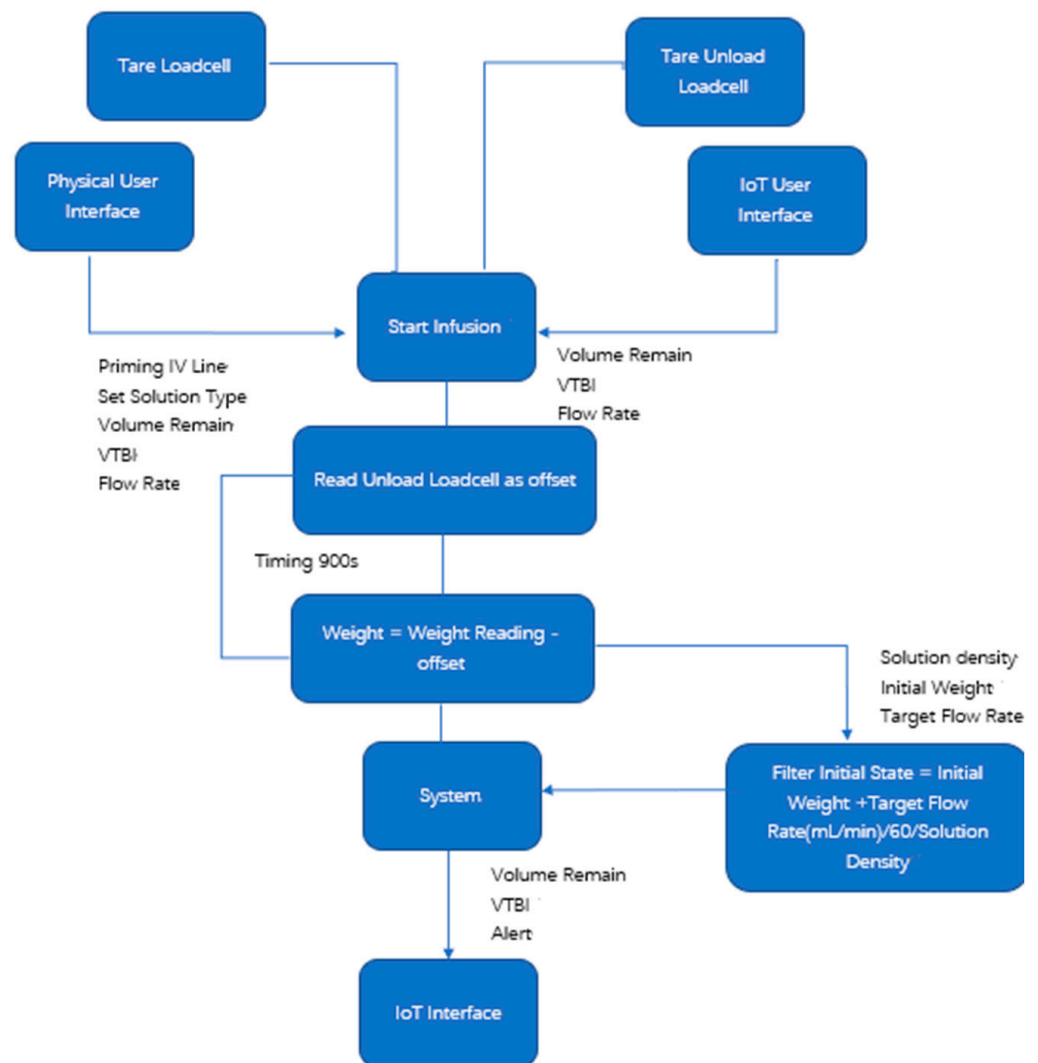


Figure 11. Block diagram of calibration process and integration with IoT.

Both load cells are working while the system power is turned on. Some parameters can be set through both the physical user interface and the IoT user interface. But some critical operations, like priming the IV line and setting the solution type, must be carried out through the physical user interface to avoid human errors. Once all the required parameters are set, the infusion can start. When the infusion begins, the MCU first reads the unload load cell to determine the offset. All weight readings subtract this offset to obtain the calibrated reading. The offset updates every 900 s to reduce the task resource consumption. Since the sensor reads weight, not volume, the readings also need to be divided by the solution density to convert it to the volume. The initial state of the IIR filter is based on the initial weight reading plus the weight of the fluid expected to flow out in one second at the set flow rate, ensuring that the flow rate input to the PI controller is close to the correct rate initially. The calculated remaining fluid volume, the VTBI, and any alerts in case of abnormal conditions are displayed in real time on the IoT user interface.

The IoT functionality is achieved through the Blynk IoT [42]. Blynk is designed with multiple layers of data security to ensure user safety and device control integrity. The application encrypts every message, providing a secure transmission, though some hardware without TLS support may not benefit from this feature. Additionally, it uses granular permission to manage who can view devices and their data [43]. As shown in Figure 12, users can set the total injection volume and flow rate through the interface and monitor the volume remaining and progress. However, the solution type must be entered from the device's physical operation panel with medical personnel present for verification.



Figure 12. Mobile Blynk IoT user interface.

4. Result

4.1. Reading Drift

Figure 13 shows the unfiltered and filtered results of the reading drift over time when the improved weighing platform is unloaded. It can be observed that the filter significantly reduces the noise level. The measured results no longer show a significant shift after 5×10^4 s, confirming the previous speculation that the shift was caused by creep. The unfiltered data's noise level is significantly higher than in previous experiments, with an unclear noise source, speculated to be due to differences in the adjustable power supply and ground condition.

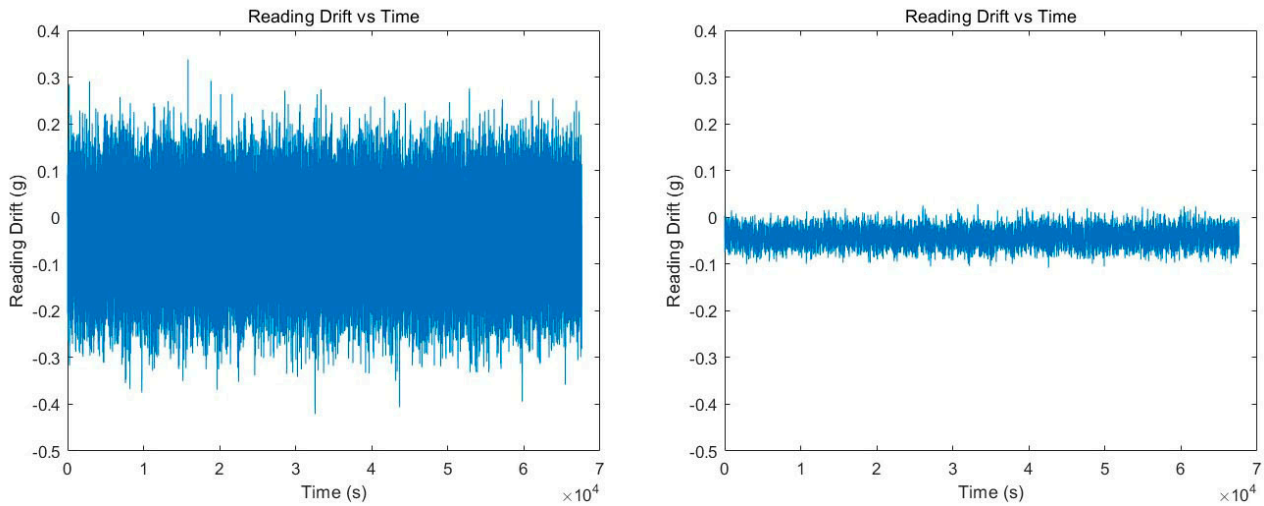


Figure 13. Unfiltered (Left) and filtered (Right) reading drift with no load.

The long-term stability and stability under multiple times of power on-off are crucial for system performance. Figure 14 illustrates the long-term stability of the weighing sensor with the filter configured. As the filter requires time to set, the readings are taken 5 min after bootup. The error in readings after bootup remains within the sensor's self-drift error, indicating that the sensor's performance has virtually not changed over a 60-day period.

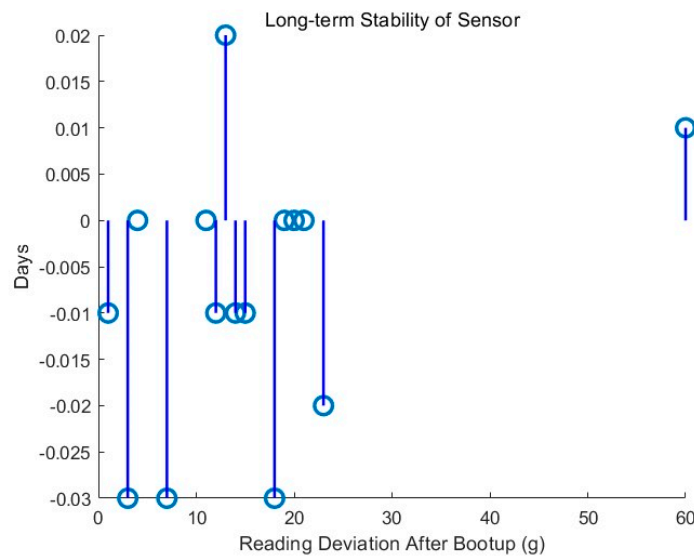


Figure 14. Reading deviation after bootup vs. days.

For multiple power cycles, the readings were recorded for 100 times of power on-off, each taken at 5 min after bootup. The standard deviation was 0.0159 g, which is also within the sensor's self-drift error, showing no unexpected results.

4.2. Flow Rate Reading Accuracy

Figure 15 displays the flow rate of the saline solution read using the filtered data from the weighing platform. The flow rate is generated by a peristaltic pump with a resolution of $0.12 \mu\text{L}/\text{min}$ and an accuracy of 0.5%. The flow rate is set to $0.1 \text{ mL}/\text{min}$, with a total volume of 50 mL.

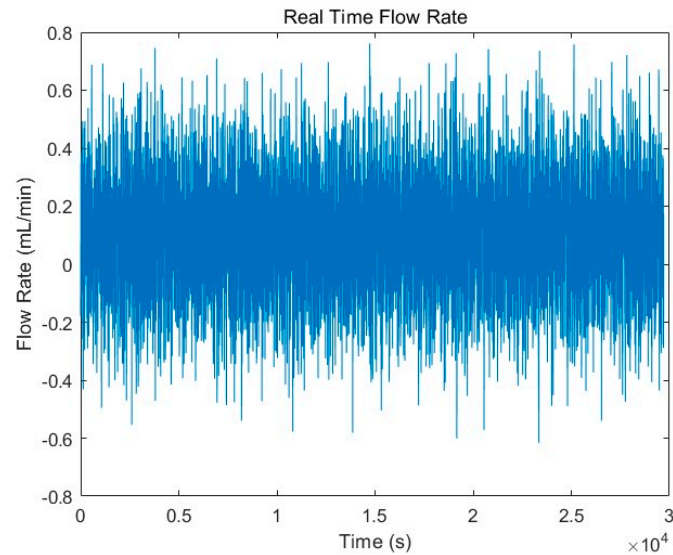


Figure 15. 0.1 mL/min actual flow rate reading.

Significant noise level increases are observed in practical applications, possibly due to the pump's vibrations coupling to the sensor. The noise in the flow rate reading is very high, making it impossible to correctly read the real-time flow rate. According to the closed-loop system modeling, the simulated cumulative error (the global flow rate error) in the PI control is 1.5%, which is within an acceptable range. However, without the self-calibration algorithm, the static data collected and filtered through the same parameter filter result in a simulated PI controller cumulative error of 15.9%. This shows that the calibration method significantly improves the global flow rate error in closed-loop control using the weight sensor to read flow rates, but whether local flow rate errors will pose problems in practical applications requires further study. When the flow rate is set to $0.5 \text{ mL}/\text{min}$, the read flow rate is as shown in Figure 16. The real-time flow display still lacks reference values, with a simulated PI controller cumulative error of 0.6%.

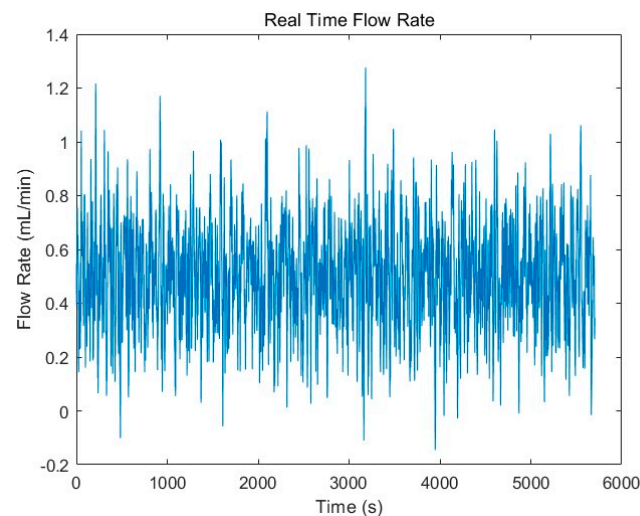


Figure 16. 0.5 mL/min actual flow rate reading.

When the flow rate is set to 1 mL/min, the read flow rate is as shown in Figure 17. The real-time flow has some reference values, but, at times, the error is still very large. The simulated PI controller cumulative error is 1.3%. The error rate has significantly increased compared to 0.5 mL/min, speculated to be due to the greater vibration disturbances caused by the increased speed of the peristaltic pump.

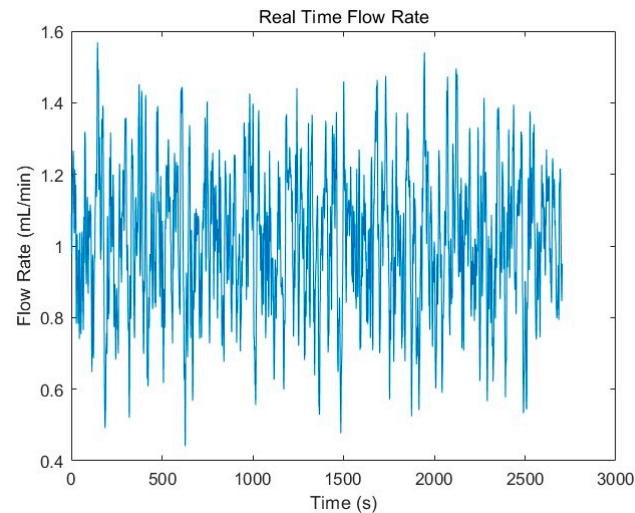


Figure 17. 1 mL/min actual flow rate reading.

For the 1 mL/min flow rate, the RMS noise is 0.1926 mL/min, and the maximum deviation is 0.5722 mL/min. For the 0.5 mL/min flow rate, the RMS noise is 0.1888 mL/min, and the maximum deviation is 0.7131 mL/min. For the 0.1 mL/min flow rate, the RMS noise is 0.1812 mL/min, and the maximum deviation is 0.6564 mL/min. It is evident that, for flow rates less than 0.2 mL/min, the actual data are completely obscured under the noise floor, despite the application of anti-aliasing filters and IIR filters. Even for a higher flow rate like 1 mL/min, the readings still have a noise-induced uncertainty of about $\pm 20\%$. In contrast, the opposed laser photoelectric sensor noise mainly comes from the common difference and environmental impact of chamber, and typically exhibits reading errors of less than $\pm 10\%$, which is the chamber per drop accuracy, indicating a much lower noise level. Therefore, this method is considered inadequate for accurately reading real-time flow rates.

4.3. Closed-Loop Control Accuracy

All measurements are conducted in an air-conditioned environment; the temperature was adjusted to 22 °C. Table 2 lists the total volume error and global flow rate error when injecting 50 mL of saline solution in closed-loop control. Since no high-precision flowmeter is available, real-time errors are not discussed.

Table 2. Flow rate and volume accuracy.

Target Flow Rate	Global Flow Rate (mL/min)	Global Flow Rate Error	Actual Volume (mL)	Actual Volume Error
0.1 mL/min	0.10083	0.83%	49.23	1.54%
0.5 mL/min	0.50134	0.27%	49.90	0.2%
1 mL/min	1.00504	0.5%	49.85	0.3%

The global flow rate error is significantly less than the simulated controller error previously, possibly due to the peristaltic pump's own errors and errors in the density calibration data. Table 3 shows the total volume error and global flow rate error when injecting 50 mL of saline solution using a method that achieves the closed-loop control of the flow rate by detecting the fluid droplets falling from the drip funnel with an opposed laser photoelectric sensor.

Table 3. Flow rate and volume accuracy for opposed laser photoelectric sensor.

Target Flow Rate	Global Flow Rate (mL/min)	Global Flow Rate Error	Actual Volume (mL)	Actual Volume Error
0.1 mL/min	0.09665	3.34%	48.30	3.4%
0.5 mL/min	0.53294	6.59%	53.25	6.5%
1 mL/min	1.03961	3.96%	52.05	4.1%

Although this method achieves an accuracy that is sufficient to meet the design requirements, the error is significantly higher than the closed-loop control implemented with the self-calibrating weight sensor. The total cost for the self-calibrating weight sensor is \$4.12, and the opposed laser photoelectric sensor costs \$3.45. Without being slightly more expensive than the photodetector, the self-calibrating weight sensor has a significant advantage in accuracy.

In a study evaluating the flow rate accuracy of six traditional IV Drip devices from different manufacturers, it was noted that, when the flow rate was set to 1.667 mL/min, the flow rate errors for these devices were 6.3%, 7.6%, 8.1%, 11.3%, 12.7%, and 16.6% [44]. Compared to these given error rates, the closed-loop control accuracy of this system is significantly better than these traditional devices.

The overall setup is shown in Figures 18 and 19.

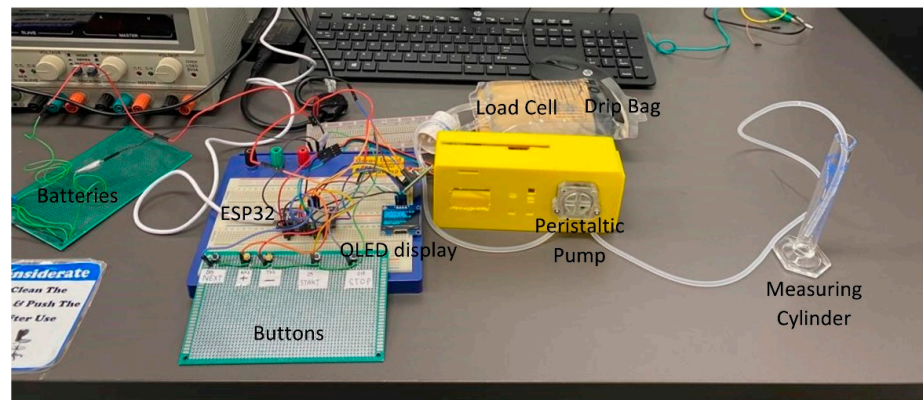


Figure 18. Overall measurement setup for weight sensor feedback.



Figure 19. Overall measurement setup for opposed laser photoelectric sensor feedback.

5. Conclusions

For smart intravenous infusion devices, achieving precise medication delivery is crucial, necessitating the sensing of the completed dosage and flow rate. This article designed an IoT-based closed-loop controlled infusion device, discussed methods for sensing the volume of fluid infused through a weight sensor, and proposed calibrating the loaded cell with the offset readings of another unloaded load cell of the same model, reading the flow rate to achieve the closed-loop control of the infusion pump. Compared to the commonly used low-cost opposed laser photoelectric sensors, this scheme partly increases the cost while significantly improving the accuracy of the global flow rate and infusion volume. Another advantage of this scheme is that the infusion device does not require a drip chamber for sensing, so it has no height requirement for the infusion set, making it more convenient for the development of home-use devices. However, this method has a significant drawback of not being able to provide accurate and reliable real-time flow rate sensing, which could be resolved by combining it with an opposed laser photoelectric sensor. Another issue is that for colloidal fluids, this method requires the calibration and standardization of different fluids' densities to achieve sufficient accuracy, thereby increasing the operational complexity. However, colloidal fluid infusions are more common in emergency scenarios and are less prevalent in the application scenarios of low-cost smart infusion devices.

Author Contributions: Conceptualization, methodology, supervision, data curation, and investigation, C.L.K.; investigation, visualization, and funding acquisition, C.K.H.; methodology, resources, and software, Y.D.; project administration, visualization, and formal analysis, T.K.L.; investigation, formal Analysis, and funding acquisition, Y.Y.K.; data curation, and formal analysis, J.P.C. All authors have read and agreed to the published version of the manuscript.

Funding: This research received no external funding.

Data Availability Statement: Data are contained within the manuscript.

Acknowledgments: The authors would like to extend their appreciation to the University of Newcastle, Australia, for financing the project and making it possible.

Conflicts of Interest: The authors declare no conflicts of interest.

References

1. Dougherty, L.; Lamb, J. Fluid and Electrolyte Balance. In *Intravenous Therapy in Nursing Practice*; Blackwell Publishing: Hoboken, NJ, USA, 2009; pp. 49–86.
2. Sonkar, A.; Pal, N.; Gupta, H.; Dhanoa, J.K. Smart Intravenous Drip Monitoring System with Bubble Detection Indicator using IoT. In Proceedings of the 2022 2nd International Conference on Intelligent Technologies (CONIT), Hubli, India, 24–26 June 2022; pp. 1–7. [CrossRef]
3. Doyle, G.R.; McCutcheon, J.A. 8.2 Intravenous Fluid Therapy. *Clinical Procedures for Safer Patient Care*. Available online: <https://opentextbc.ca/clinicalskills/chapter/intravenous-therapy-peripheral-and-central-venous-catheters/> (accessed on 26 October 2021).
4. Ray-Barruel, G.; Woods, C.; Larsen, E.N.; Marsh, N.; Ullman, A.J.; Rickard, C.M. Nurses' decision-making about intravenous administration set replacement: A qualitative study. *J. Clin. Nurs.* **2019**, *28*, 3786–3795. [CrossRef] [PubMed]
5. Hagihghi, R.; Razmjou, A.; Orooji, Y.; Warkiani, M.E.; Asadnia, M. A miniaturized piezoresistive flow sensor for real-time monitoring of intravenous infusion. *J. Biomed. Mater. Res. Part B Appl. Biomater.* **2020**, *108*, 568–576. [CrossRef] [PubMed]
6. Lueshen, E.; Tangen, K.; Mehta, A.I.; Linninger, A. Backflow-free catheters for efficient and safe convection-enhanced delivery of therapeutics. *Med. Eng. Phys.* **2017**, *45*, 15–24. [CrossRef] [PubMed]
7. Cook, L.S. Infusion-Related Air Embolism. *J. Infus. Nurs.* **2013**, *36*, 26–36. [CrossRef] [PubMed]
8. Durant, T.M.; Long, J.; Oppenheimer, M.J. Pulmonary (venous) air embolism. *Am. Heart J.* **1947**, *33*, 269–281. [CrossRef] [PubMed]
9. Sanjay, S.B.; Harish, B.; Karthikeyan, K.; Arunachalam, G.M.; Vaishnavi, K.; Anush, P.; Mahalakshmi, R. IoT Based Smart IV Drip Stand. In Proceedings of the 2021 International Conference on Advancements in Electrical, Electronics, Communication, Computing and Automation (ICAECA), Coimbatore, India, 8–9 October 2021; pp. 1–5. [CrossRef]
10. Taxis, K.; Barber, N. Causes of intravenous medication errors: An ethnographic study. *Qual. Saf. Health Care* **2003**, *12*, 343–347. [CrossRef] [PubMed]
11. Noon, K.; Poree, L.R.; Ike, K.; Jones, R.C.W. Intrathecal Pump Malfunction: Flipped, Expired, Stalled, and Malfunctioned Valves and Rotors Leading to Under- and Over-Infusion. *Challenging Cases Complicat. Manag. Pain Med.* **2018**, 181–187. [CrossRef]

12. Philip, N.Y.; Rodrigues, J.J.P.C.; Wang, H.; Fong, S.J.; Chen, J. Internet of Things for In-Home Health Monitoring Systems: Current Advances, Challenges and Future Directions. *IEEE J. Sel. Areas Commun.* **2021**, *39*, 300–310. [CrossRef]
13. Hoa, N.D. Smart Sensors for Health Care Application: Challenges and Opportunities: Keynote Talk #1. In Proceedings of the 2020 4th International Conference on Recent Advances in Signal Processing, Telecommunications & Computing (SigTelCom), Hanoi, Vietnam, 28–29 August 2020. [CrossRef]
14. Hu, H.-W.; Chih-Hao, L.; Du, Y.-C.; Chen, K.-Y.; Lin, H.-M.; Lin, C.-C. Clinical validation of a real-time medical internet of things system for detecting blood leakage during hemodialysis: A pilot study (Preprint). *JMIR Form. Res.* **2021**. [CrossRef]
15. Zhang, Y.; Zhang, S.; Ji, Y.; Wu, G. Intravenous infusion monitoring system based on WSN. In Proceedings of the IET International Conference on Wireless Sensor Network 2010 (IET-WSN 2010), Beijing, China, 15–17 November 2010; pp. 38–42. [CrossRef]
16. Saumon, G.; Loiseau, A.; Delavault, E. Servo-controlled air pump for calibration of respiratory measurement systems. *J. Biomed. Eng.* **1985**, *7*, 132–136. [CrossRef]
17. Kim, H.; Cheon, D.; Lim, J.; Nam, K. Robust Flow Control of a Syringe Pump Based on Dual-Loop Disturbance Observers. *IEEE Access* **2019**, *7*, 135427–135438. [CrossRef]
18. Jianwen, C.; Han, Z. Design of intravenous infusion monitoring and alarm system based on wireless communication technology. In Proceedings of the 2011 IEEE International Conference on Mechatronics and Automation, Beijing, China, 7–10 August 2011; pp. 130–134. [CrossRef]
19. Golden, D.J.; Castaneda, P.; Carius, B.M.; Simmons, C.J. Comparison of DripAssist to Traditional Method for Achieving Rate Infusions by U.S. Army Medics. *J. Spec. Oper. Med.* **2023**. [CrossRef] [PubMed]
20. Zargar, Z.H.; Islam, T. A Novel Cross-Capacitive Sensor for Noncontact Microdroplet Detection. *IEEE Trans. Ind. Electron.* **2018**, *66*, 4759–4766. [CrossRef]
21. Le, T.H.; Ngo, P.T.; Tran, V.N.; Tran, V.H. Liquid Level Detection via Node-Red and Automatic Image Processing System. *J. Adv. Eng. Comput.* **2022**, *6*, 73–84. [CrossRef]
22. Yu, Q. Study on monitoring infusion rate based on computer vision. *Highlights Sci. Eng. Technol.* **2023**, *63*, 33–40. [CrossRef]
23. Song, S.; Yan, S.; Zhang, S.; Jiang, Y.; Luo, H.; Ma, L. Design of an Infusion Monitoring System Based On Image Processing. *J. Phys. Conf. Ser.* **2021**, *2037*, 012109. [CrossRef]
24. Giaquinto, N.; Scarpetta, M.; Ragolia, M.A.; Pappalardi, P. Real-time drip infusion monitoring through a computer vision system. In Proceedings of the 2020 IEEE International Symposium on Medical Measurements and Applications (MeMeA), Bari, Italy, 1 June–1 July 2020; pp. 1–5. [CrossRef]
25. Blakeborough, A.; Clément, D.; Williams, M.S.; Woodward, N. Novel load cell for measuring axial force, shear force, and bending movement in large-scale structural experiments. *Exp. Mech.* **2002**, *42*, 115–122. [CrossRef]
26. Paulsen, A.W.; Ruskin, K.J. Intravenous Infusion Devices for Perioperative Use. Available online: <https://www.uptodate.com/contents/intravenous-infusion-devices-for-perioperative-use> (accessed on 16 March 2024).
27. Common Types of Loadcells. Available online: <https://www.anyload.com/common-types-of-load-cells/> (accessed on 29 February 2024).
28. Barlow, A.; Barlow, B.; Tang, N.; Shah, B.M.; King, A.E. Intravenous Fluid Management in Critically Ill Adults: A Review. *Crit. Care Nurse* **2020**, *40*, e17–e27. [CrossRef] [PubMed]
29. SJH/SJE Critical Care Intravenous Medication Chart. Uoflhealthnetwork. Available online: <https://www.uoflhealthnetwork.org/documents/IVDripNEW.pdf> (accessed on 22 October 2023).
30. Adult Critical Care IV Medication Infusion Sheet. University of Illinois Medical Center. Available online: <https://chicago.medicine.uic.edu/wp-content/uploads/sites/6/2017/09/criticalcaresdrugs.pdf> (accessed on 22 October 2023).
31. Standard and Maximum Allowable Concentrations, Guidelines for Continuous or Titrated Infusions. Adult Intravenous Medications. Available online: https://med.umkc.edu/docs/em/iv_med_reference.pdf (accessed on 22 October 2023).
32. Adult iv Push/Infusion Guidelines for Select Medications. Specialove. Available online: <https://specialove.org/wp-content/uploads/2019/08/IVPushInfusionGuidelines.pdf> (accessed on 22 October 2023).
33. Brooks, R.J.; Wilson, A.M. Simplifying infusion calculations. *BMJ* **1985**, *290*, 291–292. [CrossRef]
34. Pardeshi, N.N.; Qi, W.; Dahl, K.; Caplan, L.; Carpenter, J.F. Microparticles and Nanoparticles Delivered in Intravenous Saline and in an Intravenous Solution of a Therapeutic Antibody Product. *J. Pharm. Sci.* **2017**, *106*, 511–520. [CrossRef]
35. Load Cell + hx711 = Drifting Value. Mikgol. Available online: <https://forum.arduino.cc/t/load-cell-hx711-drifting-value/387365> (accessed on 20 January 2024).
36. How to Get More Accurate Reading Out of Load Cells with HX711. MikeLemon. Available online: <https://forum.arduino.cc/t/how-to-get-more-accurate-reading-out-of-load-cells-with-hx711/500770> (accessed on 20 January 2024).
37. HX711 Drift. OO999. Available online: <https://github.com/bogde/HX711/issues/51> (accessed on 20 January 2024).
38. Can't Get the hx711 to Return Stable Data. Bdsafa. Available online: <https://forum.arduino.cc/t/cant-get-the-hx711-to-return-stable-data/560726/5> (accessed on 20 January 2024).
39. A Reference Design for High-Performance, Low-Cost Weigh Scales. Colm Slattery and Mariah Nie. Available online: <https://www.analog.com/en/resources/analog-dialogue/articles/a-reference-design-for-weigh-scales.html> (accessed on 20 January 2024).
40. Makabe, M.; Kohashi, T. High accurate Creep compensation method for Load Cell. In Proceedings of the SICE Annual Conference 2007, Takamatsu, Japan, 17–20 September 2007; pp. 29–36. [CrossRef]

41. Wikipedia. Infinite Impulse Response. Available online: https://en.wikipedia.org/wiki/Infinite_impulse_response (accessed on 20 January 2024).
42. Blynk. A Low-Code IoT Software Platform for Business. Available online: <https://www.blynk.io/> (accessed on 20 October 2023).
43. Veal, D.F.; Altman, C.E.; McKinnon, B.T.; Fillingim, O. Evaluation of flow rates for six disposable infusion devices. *Am. J. Health Pharm.* **1995**, *52*, 500–504. [[CrossRef](#)] [[PubMed](#)]
44. Blynk. Security. Available online: <https://docs.blynk.io/en/blynk.cloud/security> (accessed on 25 April 2024).

Disclaimer/Publisher’s Note: The statements, opinions and data contained in all publications are solely those of the individual author(s) and contributor(s) and not of MDPI and/or the editor(s). MDPI and/or the editor(s) disclaim responsibility for any injury to people or property resulting from any ideas, methods, instructions or products referred to in the content.